Co-funded by the
Erasmus+ Programme
of the European Union

BIOART
Engineering education
for human welfare

PETER ARRAS AND DAVID LUENGO (EDS.)

TEACHING AND SUBJECTS ON BIO-MEDICAL ENGINEERING

APPROACHES AND EXPERIENCES FROM THE BIOART-PROJECT

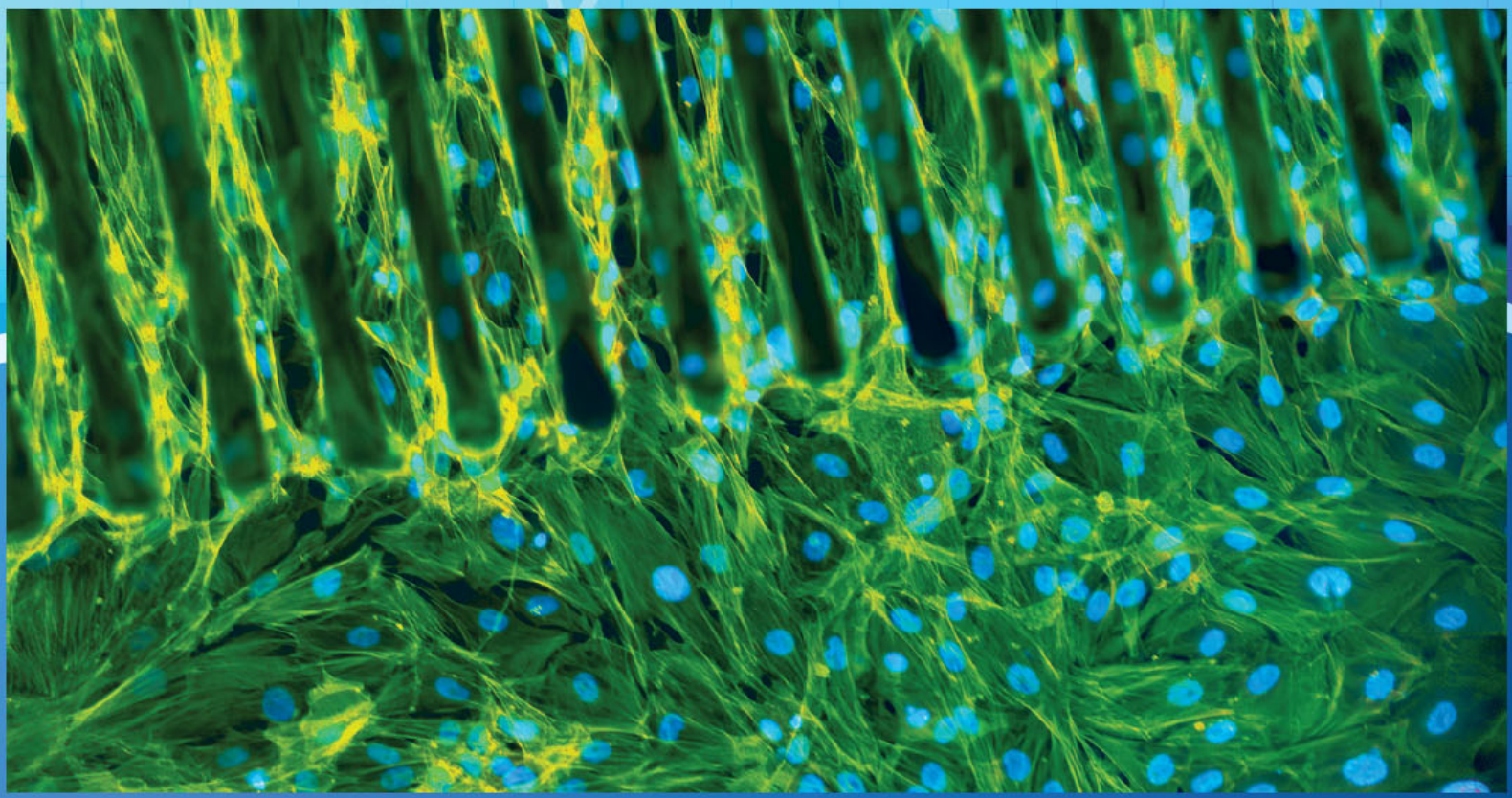

2021

Co-funded by the
Erasmus+ Programme
of the European Union

BIOART
Engineering education
for human welfare

PETER ARRAS AND DAVID LUENGO (EDS.)

TEACHING AND SUBJECTS ON BIO-MEDICAL ENGINEERING

APPROACHES AND EXPERIENCES FROM THE BIOART-PROJECT

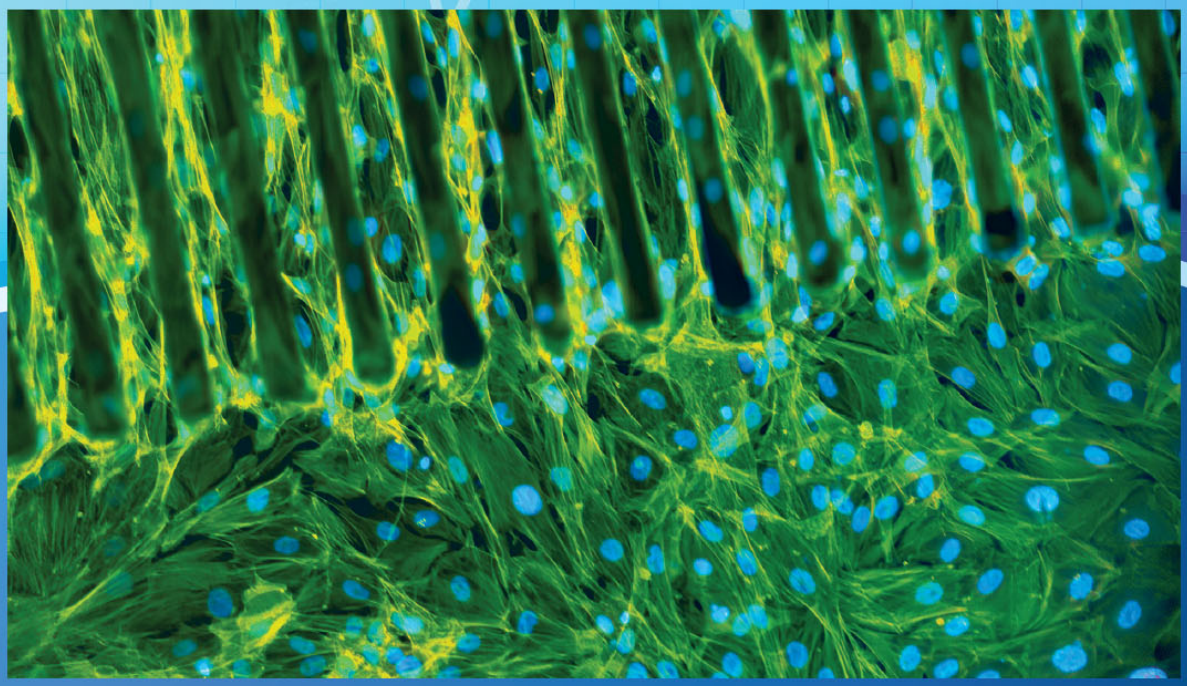

2021

Teaching and subjects on bio-medical engineering

Approaches and experiences from the BIOART-project

Peter Arras and David Luengo (Eds.)

ISBN: 978-94-641-4245-7

Keywords: Bio-medical Engineering, BIOART, implants

Cover Design: Andreiev M.O.

Cover photo: Picture by Rosalba M. Ferraro & Miriam Seiti, AML group KU Leuven in partnership with UniBs: “Cell Culturing on Patterned Substrates for Morphological Stimulation in Neural Tissue Engineering”.

First edition: 2021

The BIOART-project (Innovative Multidisciplinary Curriculum in Artificial Implants for Bio-Engineering BSc/MSc Degrees), 586114-EPP-1-2017-1-ES-EPPKA2-CBHE-JP, has been funded with the support of the Education, Audiovisual and Culture Executive Agency of the European Commission.

The European Commission’s support for the production of this publication does not constitute an endorsement of the contents, which reflect the views only of the authors, and the Commission cannot be held responsible for any use which may be made of the information contained therein.

It is shown that the application of prototyping technologies allows to improve the efficiency of the development process by reducing the design time, the number of errors and provides opportunities to improve the functional characteristics, shape, weight, and dimensions of the designed biomedical products.

References

1. Dorrier, J.: Bionic athletes with exoskeletons, robotic limbs, and brain-control devices to compete in cybathlon, https://singularityhub.com/2014/04/23/bionic-athletes-with-exoskeletons-robotic-limbs-and-brain-control-devices-to-compete-in-2016-cybathlon, last accessed 2020/12/10.
2. Mardonova, M., Choi Y.: Review of wearable device technology and its applications to the mining industry. Energies 11(3), 14 p. (2018).
3. Parkhomenko, A., Gladkova, O., Zalyubovskiy, Y.: Investigation and realization of prototyping technologies for robotic-prostheses computer aided design. In: Proceedings of XV International Conference on The Experience of Designing and Application of CAD Systems in Microelectronics (CADSM 2019), pp. 7/5-7/8. IEEE, Los Alamitos, USA (2019).
4. Liou, W.F.: Rapid prototyping and engineering applications: a toolbox for prototype development. CRC Press Taylor & Francis Group Boca Raton, 592 p. (2007).
5. McEwen, A., Cassimally, H.: Designing the Internet of things. Wiley, 338 p. (2014).
6. Belter, T.J., Segil, L.J., Aaron, M.D., Weir, F.R.: Mechanical design and performance specifications of anthropomorphic prosthetic hands. Journal of Rehabilitation Research & Development, 599-618 (2013).
7. Gaget, L.: 2018 Top 8 of the best parametric modeling software in 2020, https://www.sculpteo.com/blog/2018/03/07/top-8-of-the-best-parametric-modelingsoftware/, last accessed 2020/12/10.
8. Parkhomenko, A., Presaizen, Y., Gladkova, O., Tulenkov, A., Kalinina M.: Remote heart rate monitoring of the hospital patients. In: Proceedings of the 2019 10th IEEE International Conference on Intelligent Data Acquisition and Advanced Computing Systems: Technology and Applications (IDAACS 2019) pp. 991-996. IEEE, Los Alamitos, USA (2019).
9. Parkhomenko, A., Volynska, A., Zalyubovskiy, Y., Parkhomenko, A., Kalinina M.: Method of monitoring of young athletes' physical state indicators based on wearable devices usage. In: CEUR Workshop Proceedings, 2608, pp. 436-449. CEUR, M. Jeusfeld c/o Redaktion Sun SITE, Informatik V, RWTH Aachen, Germany (2020).
10. How we'll invent the future, by Bill Gates. MIT technology Review, February, 2019, https://www.technologyreview.com/lists/technologies/2019/, last accessed 2020/12/10.
11. Tulenkov, A., Parkhomenko, A., Sokolyanskii, A., Stepanenko, A., Zalyubovskiy, Y.: The features of wireless technologies application for Smart House systems. In: Proceedings of the 4th IEEE International Symposium on Wireless Systems within the IEEE International Conferences on Intelligent Data Acquisition and Advanced Computing Systems, pp.1-6. IEEE, Los Alamitos, USA (2018).

System of three-dimensional human face images formation for plastic and reconstructive medicine

Sergii Pavlov[1] [0000-0002-0051-5560], Oleg Avrunin[2][0000-0002-6312-687X], Oleksandr Hrushko[3][0000-0001-5551-375X], Yana Nosova[4][0000-0003-4310-5833], Natalia Shushlyapina[5][0000-0001-8958-3270]

[1, 3] Vinnytsia National Technical University, 21021, Vinnytsia, Khmelnytske shose 95, Ukraine

[2]Kharkiv National University of Radio Electronics, 61166, Nauki Ave. 14, Kharkiv, Ukraine

[4,5]Kharkiv National Medical University, 61022, Nauki Ave. 4, Kharkiv, Ukraine

[1]psv@vntu.edu.ua

[2]oleh.avrunin@nure.ua

[3]grushko1alex@gmail.com

[4]yana.nosova@nure.ua

[5]schusha75@ukr.net

Abstract. Improving the methods and means of computer planning of functional and aesthetic interventions on the human face based on realistic 3D visualization methods is an urgent task of modern biomedical engineering. Despite a sufficient amount of work in the field of medical imaging and image processing, a more accurate and realistic presentation of data is needed for imaging systems aimed at modifying the initial data to predict the results of surgery. Software for 3D visualization in computer modeling of functional and aesthetic surgical interventions should ensure the solution of the following set of tasks: initial computer processing of tomographic data and 3D surface scanning data; selection of a visualization window and tone mapping; segmentation of anatomical structures on tomographic images; determination of the contours of segmented objects on tomographic images; construction and visualization of polygonal models of the anatomical structures of the investigated area.

Keywords: Surface Scanning, Tomographic Images, Visualization.

1 Introduction

An increase in the efficiency of preoperative planning of plastic interventions can be achieved through the use of 3D visualization methods and modeling of

the deformation of structures subject to plastic correction with maximum realism. Initial data for such visualization can be obtained as a result of tomographic studies of internal structures and surface 3D scanning. In accordance with this, software systems should be developed that allow for realistic visualization and correction of the obtained 3D images, taking into account the biophysical properties of the operated area [1,2].

The wide application of this approach requires the use of universal (non-specialized) computer systems. This achieves the flexibility of improving and expanding the capabilities of software for planning operations in rhino surgery [3,4,5].

Creation of three-dimensional computer models of the human head precedes the stage of modelling changes in various anatomical parts of the head in order to obtain an optimal model corresponding to the wishes of the patient and the capabilities of the surgeon [6,7,8]. Such modeling requires the development of segmentation algorithms, complex or separate visualization and virtual deformation of anatomical structures.

2 Analysis of literary sources

Improving the methods and means of computer planning of functional and aesthetic interventions on the human face based on realistic 3D visualization methods is an urgent task of modern biomedical engineering.

The purpose of considering the features of the developed models and methods is to create a concept for the presentation, processing and analysis of tomographic data for computer planning systems in functional-aesthetic rhinosurgery.

Analysis of literature sources showed that, despite a sufficient number of works in the field of medical imaging [1,8] and image processing [9,10,11], a more accurate and realistic presentation of data is needed for imaging systems aimed at modifying the initial data to predict the results of surgery [12,13,14].

Software for 3D visualization in computer modeling of functional and aesthetic surgical interventions should provide a solution to the following set of tasks:

- initial computer processing of tomographic data and 3D surface scanning data;

- selection of the visualization window and carrying out tone mapping;
- segmentation of anatomical structures on tomographic images;
- determination of the contours of segmented objects on tomographic images;
- construction and visualization of polygonal models of the anatomical structures of the investigated area [15,16,17].

The main source of input data for the operation of the software for planning functional-aesthetic surgeries is a set of images of tomographic slices (DataSet) [1], represented as a series of files in DICOM (Digital Imaging and Communications in Medicine) format. The DICOM format is a standard for the generation, storage and transmission of radiological images and other medical information. This format, in addition to the direct results of an introscopic examination, contains data about the patient, the conditions of the study, data about the medical institution, the operators of medical equipment, the technical characteristics of the introscopic devices, the values of the physical fields underlying the study, etc. The standard enables digital interconnection between different diagnostic and therapeutic equipment from different manufacturers.

In a DICOM file, information about the study performed is stored as a set of information elements - special information structures that can store data about the patient, the study being carried out, and diagnostic equipment. The order of the elements of the tomographic dataset is such that as the element address increases, first the voxel number in the line increases, then the line number, and then the number of the slice in the axial projection [18,19,20].

3 Preliminary data preparation

Computed tomography images are gray-scale. Each slice element determines the average value of X-ray absorption in the corresponding area of the object under study during tomography. Such a 2D dataset can also be represented as anarray of brightnessor discrete intensity function, where x, y, and z are integer variables defining voxel coordinates. The domain of the function V is:

$$\begin{cases} x \in [0..w-1], \\ y \in [0..h-1], \\ z \in [0..d-1]; \end{cases} \quad (1)$$

where *w, h, d* are the sizes of the dataset in voxels.

The function V takes non-negative integer values in the range $[0 \ldots V_{MAX}]$. The value V_{MAX} depends on the bit depth N of the dataset and is determined by the formula

$$V_{MAX} = 2^N - 1 \quad (2)$$

In turn, the number of bits allocated for encoding the brightness of one element of the tomographic raster N usually takes values from 8 to 16, depending on the tomograph and the study protocol. Thus, one voxel can occupy 1 or 2 bytes in computer memory, which significantly complicates the effective processing of tomographic data and requires writing software implementations for both voxel bit widths and using generalized programming principles [21,22,23].

If the number of bits per one voxel of the initial tomographic data is not a multiple of 8, then it is advisable to round this value to the nearest higher multiple of 8, since This approach will greatly simplify the addressing of the brightness values of the voxels of the dataset and will make the software processing of tomographic data faster.

Storing tomographic slices in PC memory can require significant amounts of RAM. The content of all voxels in one memory block is preferable from the point of view of convenience and speed of programmatic access to dataset elements. However, this approach with sequential storage of voxels is not always possible due to the fact that the program may fail when allocating memory necessary to store the entire dataset in a single block. Therefore, when developing software for processing tomographic slices, it is advisable to implement the data loading algorithm in such a way that, in the event of a failure on a new memory block requested from the operating system, memory allocation is performed for each slice separately [24,25,26].

The most used strategies for storing tomographic data in RAM are slice-by-slice storage of elements and storage of elements in cubic blocks, as shown in Fig. 1.

The slice-by-cut arrangement of elements in memory involves storing raster lines sequentially one after another. The pixels in a row are stored linearly in ascending order of the x coordinate in the row. The element next to the last pixel in a line in memory is the first element of the next line. The

advantage of this way of storing voxels is the simplicity of addressing an arbitrary element of the dataset.

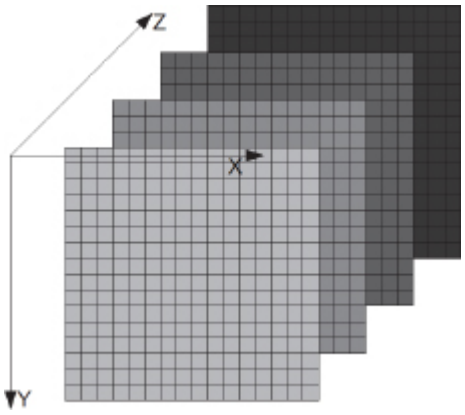

Fig. 1. Cut-by-slice presentation of tomographic study data (w=h=16, number of slices - 4).

The address of the voxel in RAM, depending on its coordinates (x, y, z), is easily calculated in accordance with the following expression:

$$Pnt_{AxVox}(x, y, z) = Pnt_{Slice}(z) + (y \cdot w + x) \cdot C(b) \quad (3)$$

where $Pnt_{Slice}(z)$ is the function that determines the memory address of the beginning of the z-th axial slice;
w - the width of the dataset in voxels;
b is the number of bits used to encode one voxel;
$C(b)$ is a function that returns the number of bytes required to store b bits, i.e. rounding b to 8 upwards, and

$$C(b) = \left(\left\lfloor \frac{(b-1)}{8} \right\rfloor + 1 \right) \quad (4)$$

When storing a dataset as a set of cubic blocks (see Fig. 2), all voxels are combined into smaller volumes with dimensions (D_X,D_Y,D_Z). Reading voxels located inside a block is also performed by progressive scanning, but within the block, not a slice. Access to the elements of the dataset with a block structure is performed in accordance with the expression

$$Pnt_{Vox}(x,y,z) = Pnt_{Slice}\left(\left\lfloor\frac{z}{D_Z}\right\rfloor\right) + \left(\left\lfloor\frac{y}{D_Y}\right\rfloor \cdot \left\lceil\frac{w}{D_X}\right\rceil + \left\lfloor\frac{x}{D_X}\right\rfloor\right) \cdot D_X \cdot D_Y \cdot D_Z \cdot C(b) + \begin{pmatrix} mod(z,D_Z)\cdot D_X \cdot D_Y + \\ +mod(y,D_Y)\cdot D_X + \\ +mod(x,D_X) \end{pmatrix} \cdot C(b) \quad (5)$$

where $mod(i,j)$ is a function that returns the remainder of dividing i by j.

Fig. 2. Block storage of tomographic dataset voxels ($D_X = D_Y = D_Z = 8$).

As can be seen from expressions (2) and (4), addressing an arbitrary voxel of a dataset when using a block strategy for storing bulk data requires more computations than with other storage methods, but for some tasks (for example, tracing or casting rays), this approach shows higher productivity. The general increase in the performance of algorithms that actively use the operation of fetching voxel values when dividing a dataset into blocks occurs primarily due to more efficient use of the caching mechanism by the central processor of cells stored in RAM [27,28,29].

Note also that it is possible to locally reduce the bit depth of some entire dataset blocks. So you can reduce the number of bits, which encodes the brightness of the voxels of this block, to N if the following conditions are met:

$$\begin{cases} V_{MAX} - V_{MIN} \le 2^N - 1, \\ N < M. \end{cases} \quad (6)$$

This approach also makes it possible to somewhat reduce the average access time to the elements of a three-dimensional array of tomographic data and, as a rule, significantly reduce the amount of memory required for storing the tomographic dataset as a whole. A three-dimensional array of luminosities using the described approach to storing elements is called a sparse dataset [30,31].

Storing tomographic data in the form of a sparse dataset and its corresponding software processing are in some cases the only possible effective way to work with datasets characterized by large sizes or in conditions of a small available amount of RAM.

4 Tone Mapping

The next step is tone mapping, which allows more efficient use of the dynamic range of tomographic imaging and promotes better perception of the obtained images by the operator, allows better differentiation in the image of tissues of various kinds that differ in density, and, consequently, in brightness in the output images.

In the case of linear transformation of brightness ranges during tone mapping, the brightness of an image element after I_D compression depends on the brightness of the corresponding pixel I_S in the original image according to the expression

$$I_D = W_{DL} + \frac{(I_S - W_{SL}) \cdot (W_{DR} - W_{DL})}{W_{SR} - W_{SL}} \quad (7)$$

where $[W_{DL} \ldots W_{DR}]$ is the brightness range (brightness window) used to display the image to which the tonal range has been applied;
$[W_{SL} \ldots W_{SR}]$ - the tonal range of the original image.
The results of the method according to formula (7) (see Fig. 3).

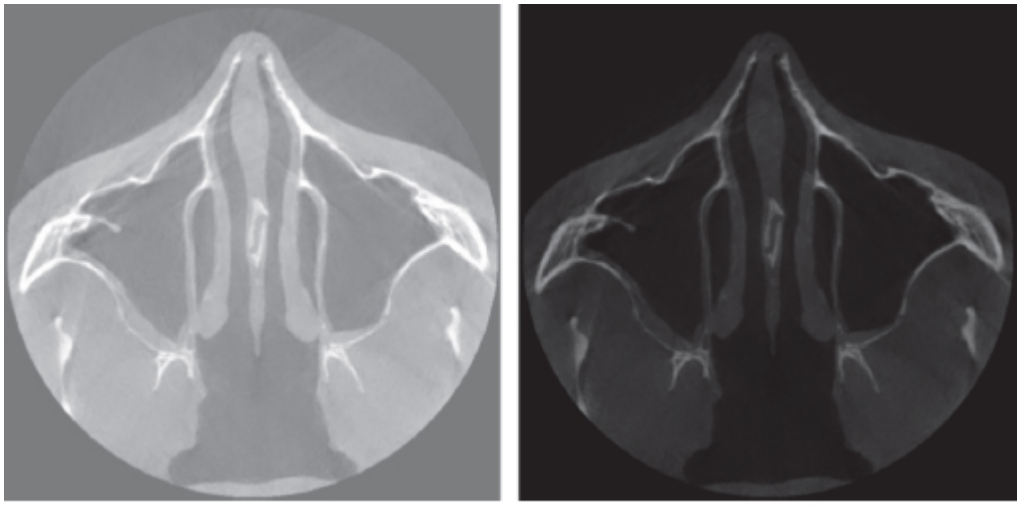

Fig. 3. Tomographic section of the patient's head: a) before tone mapping (W_{SL} = 30920, W_{SR} = 40375); b) after tone mapping (W_{DL} = 35760, W_{DR} = 44760).

5 Segmentation of Anatomical Structures

In the automated analysis of tomographic data, one of the most important operations preceding the main stages of processing the original images is the task of segmentation - determining which image pixels carry information about the amount of X-ray absorption by the object under study, and which do not belong to it. It is advisable to perform this operation by recursive filling of connected pixels that have passed binarization with a lower threshold, which will be discussed in detail below.

During the segmentation and classification of tomographic slices, an additional twodimensional array A is created for each tomographic image with the same dimensions as the raster being processed. Before the start of segmentation, all elements of this array are initialized to zero. The result of the classification of any voxel in the dataset is entering one of the nonzero values T_1, T_2 or T_3 into the cell of array A. These values are determined by the type of region to which this voxel belongs, and as a result, this voxel becomes an element of one of the following segmented sets D_1, D_2, D_3, for which

$$(x, y, z) \in D_i, \quad \text{if } A(x, y, z) = T_i \ (i = 1, 2, 3) \tag{8}$$

When binarization with a lower threshold, if the brightness of a given voxel $V(x, y, z)$ is less than or equal to a certain threshold value (V_1), then the value of the element in array A remains unchanged. If the brightness is greater than V_1, then $A(x, y, z) = T_1$. Thus, for binarization with a lower threshold, the following expression is valid:

$$A(x,y.z) = \begin{cases} T_1, & V(x,y,z) > V_1 \\ A(x,y,z), & V(x,y,z) \le V_1 \end{cases} \quad (9)$$

After isolating the background pixels of the slices, the stage of isolating and classifying the tissues of the human head on the images of tomographic slices begins using the operation of filling connected pixels that satisfy the following binarization condition with an upper threshold:

$$A(x,y.z) = \begin{cases} T_2, & V(x,y,z) < V_2 \\ A(x,y,z), & V(x,y,z) \ge V_2 \end{cases} \quad (10)$$

where V_2 is some threshold value.

Another type of threshold classification that is used at the stage of segmentation and classification of tissues imaged on tomographic sections is binarization with double limitation in accordance with the expression:

$$A(x,y,z) = \begin{cases} A(x,y,z), & V(x,y,z) \le V_1 \\ T_3, & V_2 > V(x,y,z) > V_1 \\ A(x,y,z), & V(x,y,z) \ge V_2 \end{cases} \quad (11)$$

As a result of this operation, those elements of the raster are selected, the brightness of which lies in the range. This operation can be useful, for example, when recognizing soft tissues on tomographic sections.

The first stage of the fill operation is to determine the initial (seed) pixels, starting from which the operation of growing the segmented area will take place. In the case of automated background selection on a slice image, such points are usually selected pixels located at the edges and corners of the slice, provided that their brightness is not higher than the threshold value.

If it is necessary to fill the pixels of the biological object under study, the operator chooses pixels that exactly belong to the biological object as starting points. Segmentation of the airway anatomical structures, such as the

upper airways, usually requires manual setting of the initial filling points in an interactive mode, as well as the definition of special limiters that do not allow many segmented pixels to expand through specified areas of the image (some nasal passages, anastomosis) that satisfy the threshold condition. classification.

The specified starting points of the fill are added to a special data structure that has a stack organization. This structure is necessary, since during each iteration of the filling cycle, for each processed element there can be up to 4 neighboring elements in the case of filling a four-connected area, or up to 8 neighbors in the case of processing an eight-connected environment, which are to be processed in subsequent iterations of the algorithm. By its principle of operation, a stack is similar to a queue with the only difference that the first element added to the stack will be popped last, and the last added element, on the contrary, will be the first. This difference between a queue and a stack makes it easier and more efficient to use the latter for storing image elements waiting to be processed by this segmentation algorithm with the same final result.

In case of multi-slice segmentation of a human head in a tomographic dataset, in addition to 4 or 8 pixels of this slice, which are adjacent to the considered pixel, it is also necessary to check the values of voxels having the same two-dimensional coordinates, but located on adjacent slices. This approach is used when pouring on sections of head tissue and, as a rule, makes it possible to select all the space occupied by the patient's head tissue at one time.

6 Voxel Rendering and Surface Rendering

A simpler implementation of the fill function is also possible, recursively calling itself when checking for connected pixels. If the traversal of connected areas is implemented using a regular recursive call of the subroutine for checking neighboring pixels, then with each call, the address from which this function was called, its arguments, local variables, and the current values of general-purpose registers are saved on the stack. This leads to an avalanche-like increase in the amount of used memory of the system stack and, ultimately, can lead to its overflow and, consequently, to the abnormal termination of the program. Therefore, the use of the filling algorithm using recursive calls is fraught with overflow of the system stack at

a large depth of recursion nesting and is not suitable for stable and fast segmentation of large and medium volumes of tomographic data.

It is possible to speed up the segmentation procedure for large tomographic volumes even more by using the principle of row-wise filling. The main difference between this method and the filling of connected pixels is that during one iteration of the cycle, a series of pixels are filled sequentially to the left and right of the element processed during this iteration of the fill cycle. This approach is much more efficient by processing more pixels per loop iteration, reducing the number of repetitions, and also by reducing the amount of stack used. Below is table 1 containing data reflecting the pouring processes, the stages of which are shown in Fig. 4 and 5.

The characteristics given in Table 1 prove the significant superiority of the row-byrow fill method over the four-connected pixel fill method for such tasks of processing tomographic images as highlighting the background in a tomographic image, as well as segmenting the tissues of the head and upper respiratory tract. Line-by-line filling is the most optimal not only for reasons of the general performance of the algorithm, but also because of the significantly less use of additional memory. In addition, the line-by-line pixel traversal also improves the speed of such segmentation by taking into account the organization of the CPU's cache memory. The stage of identifying the contours of anatomical structures on tomographic images is necessary for a clear morphological separation of models of these structures [32,33,34].

Table 1. Comparison of the characteristics that determine the effectiveness of the threshold segmentation algorithms when filling the background of the test slicen.

	Segmented area,%	Number of fill iterations performed	The amount of used stack memory, Bytes	Algorithm execution time, μs
Quadruple fill	10	8414	33528	1370
	40	33731	133812	3230
	70	63778	215176	5174
	100	128108	159408	9507
Line-by-line fill	10	41	12	214
	40	510	30	930
	70	1045	36	1445
	100	1225	12	1848

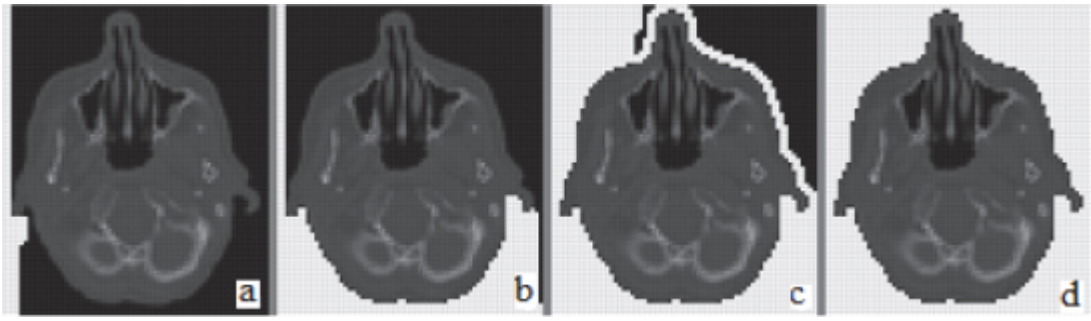

Fig. 4. Stages of selecting the background of a tomographic slice by the method of filling a fourconnected area: a) 10% of the background is filled; b) 40%; c) 70%; d) 100%.

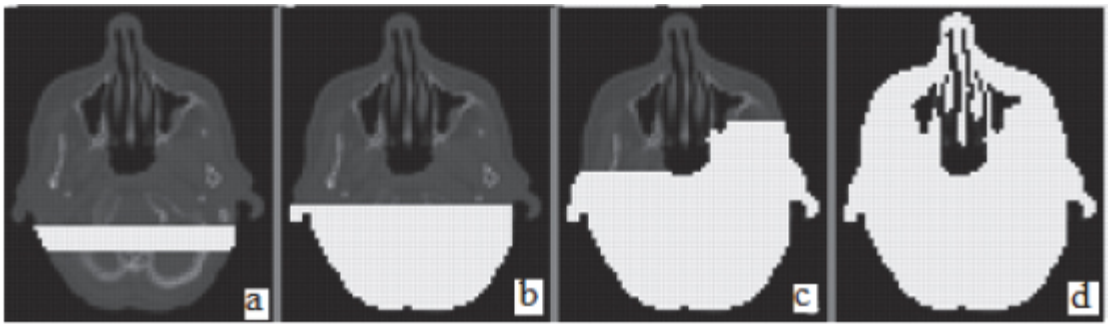

Fig. 5. Stages of separation of tissues of the human head on a tomographic section: a) 10% of the pixels of the head are filled in; b) 40%; c) 70%; d) 100%.

Algorithms of this kind make it possible to clearly distinguish morphologically on the sections of biological structures (objects) after their preliminary classification according to the necessary attribute and to form a set of segments describing a closed broken line of the contour. The information obtained at this stage about the contours of objects subsequently forms the basis of the wire 3D model.

The marking of segmented areas is necessary for the subsequent selection of the contours of the selected areas and preparation for building wire models.

At this stage, each element of the auxiliary buffer is filled according to the type of area to which it belongs. Now, in this buffer, it is necessary to select separate areas and number the segmented voxels, so that later it will be possible to determine to which area each segmented element of the tomographic data array belongs.

Further, upon completion of the stage of marking the segmented parts of the image, the pixels located on the inner border of the segmented areas are selected. Let the matrix F have the following form:

$$F = \begin{pmatrix} 1 & 1 & 1 \\ 1 & -8 & 1 \\ 1 & 1 & 1 \end{pmatrix} \quad (12)$$

A pixel is considered to be on the border of the segmented area if, during the check in the auxiliary array of its eight-connected environment by the sliding window F, the result is nonzero. This condition is true if at least one of the eight pixels surrounding the given one does not belong to the processed area.

In order not to start another additional array for storing the results of the operation of selecting the boundaries of the segmented regions, the edge pixels are marked in the previously used auxiliary array by setting a certain bit to one state. The setting of a bit can be done either by performing the "logical or" operation with the number C, or by performing the operation:

$$A'(x, y, z) = A(x, y, z) + C \quad (13)$$

moreover $A(x, y, z) < C$.

To set this bit not to affect the bits of the auxiliary array, which are responsible for encoding the segmented area number, the value of the number C must be calculated in accordance with the following formula:

$$C = 2^{[log_2 a]} \quad (14)$$

where a is the number of segmented areas in the tomographic image.

In order to build a contour model in the future, it is necessary to find a set of line segments that describe the boundaries of the selected areas. This stage begins with the creation of an array of chain codes, into which a bit mask is written, corresponding to the presence of border pixels in the eight-connected region of a certain raster element (see Fig. 6).

An array of chained codes is another auxiliary two-dimensional array, the number of rows and columns in which is the same as in the original tomographic raster. To store information about the presence or absence of a contour pixel in a certain position of an eight-connected environment, 1 bit of

information is enough. Based on this, the size of the element of the chain codes buffer from the point of view of minimizing the use of the RAM resource should be chosen equal to 1 byte.

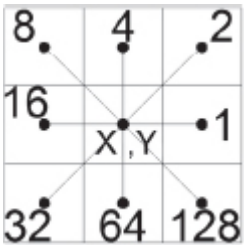

Fig. 6. The value of the bit mask of the element of chain codes, depending on the location of the associated edge pixels.

It is possible to determine the value of the chain code for a certain element of the tomographic image, based on its eight-connected environment, in accordance with the following expression:

$$B(x,y,z)=\sum_{i=0}^{7} 2^{\left\lfloor \frac{ang(x_{i-x},y_i-y)\cdot 4}{\pi} \right\rfloor} \cdot \left\lfloor \frac{A(x_i,y_i,z)}{C} \right\rfloor \qquad (15)$$

where i is the number of the pixel (x_i, y_i, z) in the array of the eight-connected environment of the considered pixel (x, y, z) (see Fig. 6);

ang (dx,dy) - function, which calculates the angle, plotted in the counterclockwise direction, between the segment given by the points (x, y), (x_i, y_i) and the horizontal ray emitted from the point (x, y) in the positive direction along the X axis;

$$ang(dx,dy)=\begin{cases} arctg\dfrac{dy}{dx}, dx>0, dy>0 \\ arctg\dfrac{dy}{dx}+\pi, dx<0 \\ arctg\dfrac{dy}{dx}+2\pi, dx>0, dy<0 \end{cases} \qquad (16)$$

where $dx = x_i - x$; $dy = y_i - y$.

The set of connected segments that form a polyline of a contour is obtained as a result of sequential traversal of nonzero elements of the array

of chain codes. If a certain pixel belongs to the contour (see Fig. 7, a) and has no more than two contour neighbors in an eight-connected area, then the centers of these pixels are connected by segments, otherwise the traversal occurs in a certain angular direction, for example, clockwise (see Fig. 7, c) in order to avoid the appearance of transverse lines that do not define the border of the segmented area (see Fig. 7, b). The resulting contour can be simplified by combining into one segment a sequential series of connected segments (see Fig. 7, d), having the same direction.

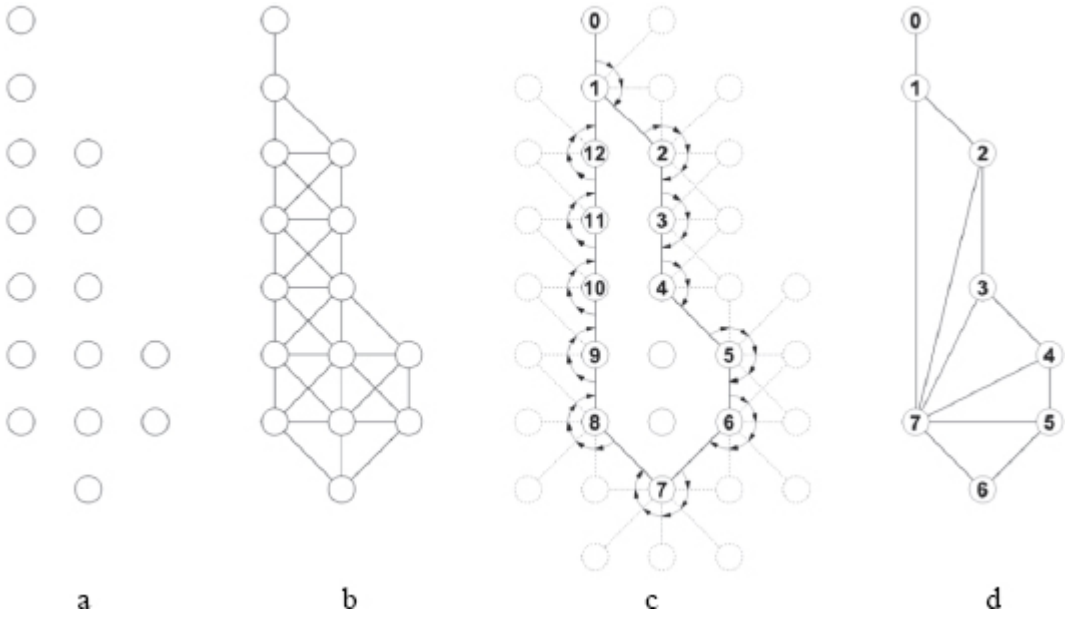

Fig. 7. Construction of a polyline based on the data of contour pixelsa) original contour pixels; b) incorrect connection of the contour nodes; c) angular traversal of contour pixels; d) the contour after its simplification and triangulation

It is considered that one segment of the contour given by the points (x_1, y_1) and (x_2, y_2) is a continuation of another segment with coordinates (x_2, y_2), (x_3, y_3) if the condition specified in the expression

$$\frac{x_2 - x_1}{y_2 - y_1} = \frac{x_3 - x_2}{y_3 - y_2} \tag{17}$$

In this way, as a rule, it is possible to achieve a significant reduction in the geometric complexity of the contour of the segmented area, which reduces

the amount of memory required for its storage, and accelerates its subsequent processing.

Having received a closed outline of the selected area, you can calculate such its characteristics as the perimeter and area. In the context of planning surgical interventions on the upper respiratory tract and the human face, this can be useful, for example, to assess the geometry of the anatomical structures of the face or to calculate the functional parameters of the patient's nasal breathing [15,16]. An illustration of the results of the algorithm for segmentation of the contours of the airways of the upper respiratory tract is shown in Fig. 8.

The advantage of the algorithm created in the work is, first of all, the lower complexity of the contours of the selected areas in the images, which simplifies and accelerates the further processing of these images, in particular, their specified contours.

By presenting a set of contours of different slices of one tomographic dataset in three-dimensional space, it is possible to form a spatial wire model (see Fig. 9, a).

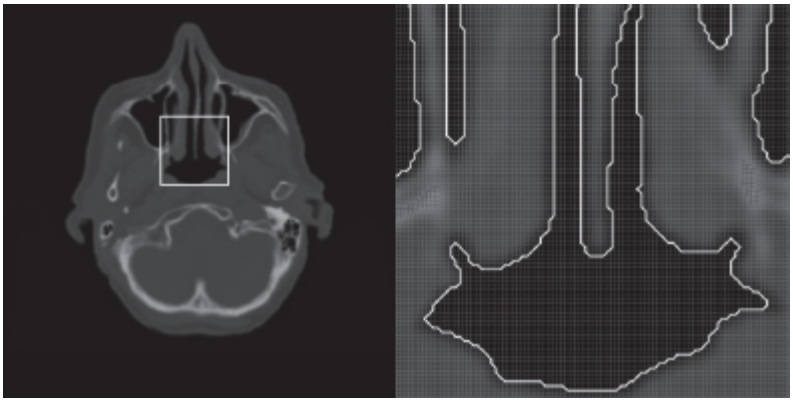

Fig. 8. Selection of the contours of the upper respiratory tract on the tomographic image: a) the processed area of the original image; b) the result of constructing a contour for a given area of the image using the proposed method

Operations such as segmentation of anatomical structures and the selection of their contours often need to be performed not only in the axial, but also in other projections (see Fig. 9, b, Fig. 9, c). In this case, the operation of multiplanar reconstruction is performed, in which the initial set of slices (usually axial) is recalculated into the same set of slices, but

corresponding to a different projection (see Fig. 10). In particular, this is necessary when calculating the geometric characteristics of the air-conducting paths of the nose based on the results of processing a series of frontal tomographic sections [13,14].

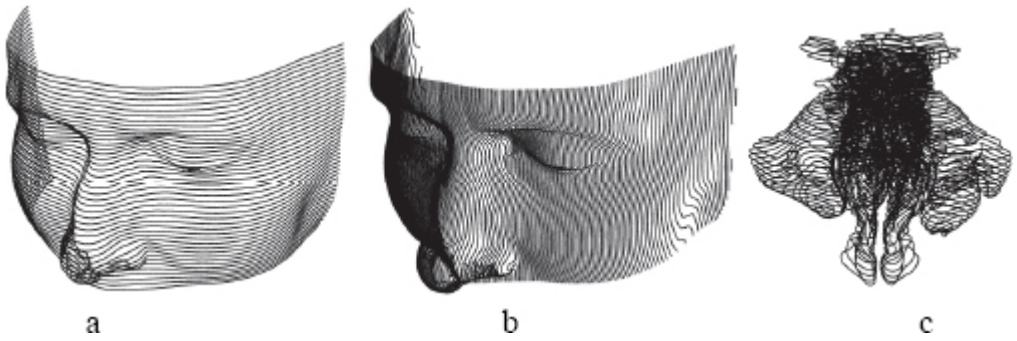

Fig. 9. Spatial contour models obtained as a result of cut-through processing of tomographic data: a) a model of the face, built from axial slices; b) a model of the face, built on sagittal sections; c) model of the upper respiratory tract.

One of the widely used methods of visualization of the studied biological objects based on the results of computed tomography is the display of voxel polygonal models. The voxel model is a three-dimensional array of the simplest volumes of the same size. When rendering a voxel model of tomographic data, each segmented element of the tomographic volume is displayed as a separate small cube (rectangular parallelepiped if the lengths of the voxel sides are not equal to one), each face of which consists of 2 triangles. Voxels that are not related to the biological object are ignored and are not displayed in 3D space. Thus, it turns out that in order to visualize one voxel in threedimensional space, it is necessary to draw 12 triangles built on 8 vertices, which makes a rather serious computational load on the block of the used graphics library, which is responsible for vertex transformations and lighting, when rendering large volumes of tomographic data. As an example, voxel models of the upper respiratory tract (see Fig. 11, a) and the human face (see Fig. 11, b) are given.

Fig. 10. Presentation of computed tomography data, segmentation results and contouring in three main projections.

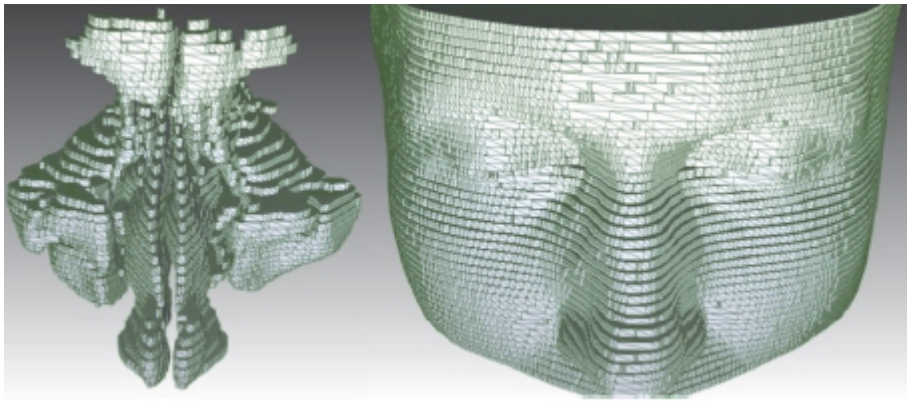

Fig. 11. Voxel models: a) model of the upper respiratory tract; b) model of the human facial region.

To render a voxel model in real time with a frame rate acceptable for visual perception, as a rule, it is necessary to perform preliminary optimization aimed at simplifying the geometry of the model, reducing the number of simple geometric shapes that describe the model (primitives). This simplification of geometry implies the elimination of individual invisible faces and entire voxels from the model, as well as combining several faces of adjacent voxels into one face (see Fig. 12).

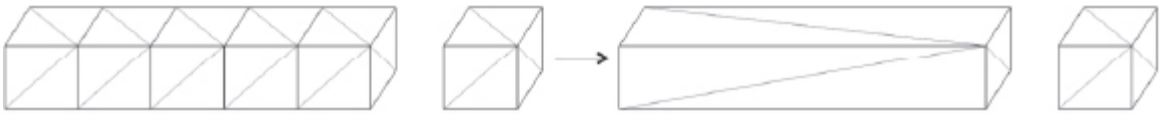

Fig. 12. Simplification of the geometric component of the voxel model by combining the faces of adjacent voxels.

The voxel representation model is quite informative for the purposes of medical diagnostics and planning of operations. It most closely matches the input tomographic data and allows you to directly calculate the geometric characteristics of the anatomical objects of the facial region and the upper respiratory tract of a person, visually assess the spatial relationships between the air cavities, nasal passages, fistulas and surrounding structures, and display the localization of the location of pathologically altered areas.

The voxel method of data visualization is quite visual, but it has a number of disadvantages: the mutually perpendicular voxel edges are not convenient for perception, and the standard lighting calculation methods applied to the model do not add depth and volume to the resulting image. The application of the “Marching Squares” algorithm [17] allows obtaining a three-dimensional surface consisting of triangles, limiting the parts of the tomographic volume that differ in brightness or segmentation mask (see Fig. 12, Fig. 13). Visualization of anatomical structures at the subvoxel level is also relevant for the study of parietal air flows in the nasal cavity [18-20].

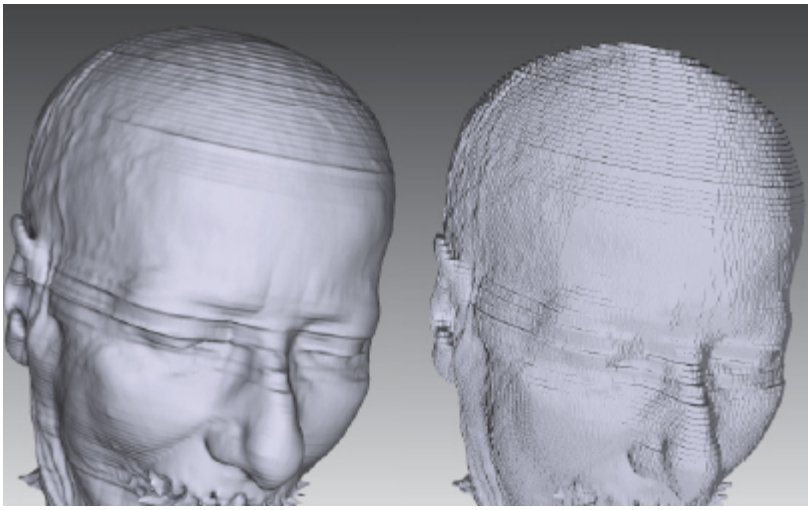

Fig. 13. Result of applying the “Marching Cubes” algorithm to a tomographic dataset 512x512x106 voxels with and without interpolation of the position of the triangle vertices.

7 Conclusions

Voxel models of tomographic data presentation are quite informative for the purposes of medical diagnostics and planning of operations. It is advisable for realistic visualization to triangulate the original voxel volume using the Marching Squares method and obtain three-dimensional surfaces that limit anatomical structures that differ in brightness or other features during segmentation.

Using modern high-speed computing systems with multi-core processors, it is possible, on the basis of the developed algorithms and software modules, to solve the problem of creating computer 3D models of the anatomical structures of the human head in real time. The created computer models are the basis for the subsequent solution of such problems: modification of 3D models in order to determine the optimal shape for the patient of certain anatomical structures subject to plastic surgery; assessment of the functioning of the upper respiratory tract and computer planning of surgical correction of intranasal structures, if necessary. The prospect of the work is the development of methods of volumetric deformation of models of the anatomical structures of the nasal cavity for the possibility of their virtual correction, taking into account the biophysical properties of the investigated area and the realism of 3D visualization.

References

1. Avrunin, O. G., Alkhorayef, M., Saied, H. F. I., &Tymkovych, M. Y. The surgical navigation system with optical position determination technology and sources of errors. Journal of Medical Imaging and Health Informatics, 5(4), 689-696 (2015).
2. Moscatiello, F., Jover, J. H., Ballester, M. A. G., Hernández, E. C., Piombino, P., &Califano, L.. Preoperative digital three-dimensional planning for rhinoplasty. Aesthetic plastic surgery, 34(2), 232-238(2010).
3. Park, S. S.. Fundamental principles in aesthetic rhinoplasty. Clinical and Experimental Otorhinolaryngology, 4(2), 55(2011).
4. Adamson, P., Smith, O., & Cole, P.. The effect of cosmetic rhinoplasty on nasal patency. The Laryngoscope, 100(4), 357-359(1990).
5. Kherani, S., Javer, A. R., Woodham, J. D., & Stevens, H. E.. Choosing a computer-assisted surgical system for sinus surgery. Journal of otolaryngology, 32(3) (2003).
6. Innis, W., Byrne, P., &Tufano, R. P.. Image-guided osteoplastic frontal sinusotomy. American journal of rhinology, 19(5), 430-434(2005).
7. Strauss, G., Koulechov, K., Richter, R., Dietz, A., Trantakis, C., &Lüth, T.. Navigated control in functional endoscopic sinus surgery. The International Journal of Medical Robotics and Computer Assisted Surgery, 1(3), 31-41 (2005).
8. Cole, P., &HollierJr, L. Use of Intraoperative CT Scanning in Endoscopic Sinus Surgery: A Preliminary Report. Journal of Craniofacial Surgery, 20(1), 265(2009).

9. Tingelhoff, K., Moral, A. I., Kunkel, M. E., Rilk, M., Wagner, I., Eichhorn, K. W., ...&Bootz, F. Comparison between manual and semi-automatic segmentation of nasal cavity and paranasal sinuses from CT images. In 2007 29th Annual International Conference of the IEEE Engineering in Medicine and Biology Society (pp. 5505-5508). IEEE. (2007).
10. Pirner, S., Tingelhoff, K., Wagner, I., Westphal, R., Rilk, M., Wahl, F. M., ...&Eichhorn, K. W. CT-based manual segmentation and evaluation of paranasal sinuses. European archives of oto-rhino-laryngology, 266(4), 507-518. (2009).
11. Tymkovych, M. Y., Avrunin, O. G., Paliy, V. G., Filzow, M., Gryshkov, O., Glasmacher, B., ...&Kozbekova, A.. Automated method for structural segmentation of nasal airways based on cone beam computed tomography. In Photonics Applications in Astronomy, Communications, Industry, and High Energy Physics Experiments 2017 (Vol. 10445, p. 104453F). International Society for Optics and Photonics. (2017, August)
12. Avrunin, O. G., Tymkovych, M. Y., Moskovko, S. P., Romanyuk, S. O., Kotyra, A., &Smailova, S. Using a priori data for segmentation anatomical structures of the brain. PrzeglądElektrotechniczny, 3, 102-105. (2017).
13. Al_Omari, A. K., Saied, H. F. I., &Avrunin, O. G.. Analysis of Changes of the Hydraulic Diameter and Determination of the Air Flow Modes in the Nasal Cavity. In Image Processing and Communications Challenges 3 (pp. 303-310). Springer, Berlin, Heidelberg. (2011).
14. Saied, H. F. I., Al_Omari, A. K., &Avrunin, O. G. An Attempt of the Determination of Aerodynamic Characteristics of Nasal Airways. In Image Processing and Communications Challenges 3 (pp. 311-322). Springer, Berlin, Heidelberg. (2011).
15. Avrunin, O. G., Nosova, Y. V., Paliy, V. G., Shushlyapina, N. O., Kalimoldayev, M., Komada, P., &Sagymbekova, A. Study of the air flow mode in the nasal cavity during a forced breath. In Photonics Applications in Astronomy, Communications, Industry, and High Energy Physics Experiments 2017 (Vol. 10445, p. 104453H). International Society for Optics and Photonics. (2017).
16. Knigavko, Y. V.. Calculation of venturi nozzles diameter for nasal breathing evaluation device. International Journal of Mechanical Engineering, 2, 21-28. (2013)
17. Newman, T. S., & Yi, H.. A survey of the marching cubes algorithm. Computers & Graphics, 30(5), 854-879. (2006)
18. Nosova, Y., Avrunin, O., Tymkovych, M., Khudaieva, S., Yurevych, N., &Glasmacher, B.. Determination of nasal breathing disorders according to computer tomography. In 2020 IEEE 40th International Conference on Electronics and Nanotechnology (ELNANO) (pp. 516-519). IEEE(2020).
19. Avrunin, O. G., Nosova, Y. V., Shushliapina, N. O., Kulish, S. M., Krekoten, E. G., Maciejewski, M., &Rakhmetullina, S.. Method for determination of laminar boundary layer of airflow in the upper respiratory tract. In Photonics Applications in Astronomy, Communications, Industry, and High-Energy Physics Experiments 2019 (Vol. 11176, p. 1117631). International Society for Optics and Photonics. (2019).
20. Nosova, Y. V., Faruk, K. I., &Avrunin, O. G. A tool for researching respiratory and olfaction disorders. Telecommunications and Radio Engineering, 77(15), 1389-1395.(2018).
21. Vyatkin Sergey, Romanyuk Alexander, Romanyuk Oksana, Nechyporuk Mykola, Troyanovskaya Tatiana and Tsikhanovska Olena. Photorealistic object reconstruction using perturbation functions and features of passive stereo projection. CONFERENCE ACIT' (2020).
22. Bezsmertnyi Y.O., Shevchuk V.I., Grushko O.V., Tymchyk S.V., Bezsmertna H.V.? Dzierżak R, et al. Information model for the evaluation of the efficiency of osteoplasty performing in case of

amputations on below knee. Proc. SPIE 10808, Photonics Applications in Astronomy, Communications, Industry and High-Energy Physics Experiments 2018, 108083H (2018).
23. Shevchuk V.I., Bezsmertnyi Y.O., Kyrychenko V.I. M'iazova plastyka pid chas amputatsii i reamputatsii homilky [Muscular plastic during amputation and abdominal shaft. Orthopedics, traumatology and prosthetics]. Ortopedija, travmatologija i protezirovanie. 4 (2010), pp. 13-18 9 (2010). (in Ukrainian).
24. Shevchuk V.I., Bezsmertnyi Y.O., Maiko V.M.. Kistkova plastyka pry amputatsiiakh ta reamputatsiiakh nyzhnikh kintsivok [Bone plastics with amputations and reamputs of the lower extremities]. Ortopedija, travmatologija i protezirovanie. 1 (2011), pp 47-55 (2011). (in Ukrainian).
25. Yurii O. Bezsmertnyi, Viktor I. Shevchuk, Sergii V. Pavlov, "Prognosis of efficacy of medical and social rehabilitation in disabled individuals with respiratory diseases", Proc. SPIE 11176, Photonics Applications in Astronomy, Communications, Industry, and High-Energy Physics Experiments 2019, 1117633 (6 November 2019); https://doi.org/10.1117/12.2537340.
26. Yurii O. Bezsmertnyi, Sergii V. Pavlov, and etc. "Information model for forecasting of violation reparative osteogenesis of long bonds", Proc. SPIE 11176, Photonics Applications in Astronomy, Communications, Industry, and High-Energy Physics Experiments 2019, 111762A (6 November 2019); https://doi.org/10.1117/12.2536250.
27. Sergey I. Vyatkin, Olexander N. Romanyuk, Sergii V. Pavlov, and etc. "Transformation of polygonal description of objects into functional specification based on three-dimensional patches of free forms", Proc. SPIE 11176, Photonics Applications in Astronomy, Communications, Industry, and High-Energy Physics Experiments 2019, 1117622 (6 November 2019); https://doi.org/10.1117/12.2537043.
28. Sergey I. Vyatkin, Olexander N. Romanyuk, Sergii V. Pavlov, and etc. Offsetting and blending with perturbation functions // Proc. SPIE 11045, Optical Fibers and Their Applications 2018, 110450W, 2019; doi: 10.1117/12.2522353; https://doi.org/10.1117/12.2522353.
29. Sergey I. Vyatkin, Olexander N. Romanyuk, Sergii V. Pavlov, and etc. A GPU-based multivolume rendering for medicine // Proc. SPIE 11045, Optical Fibers and Their Applications 2018, 1104513, 2019); doi: 10.1117/12.2522408.
30. Sergey I. Vyatkin, Olexander N. Romanyuk, Sergii V. Pavlov, and etc. Offsetting and blending with perturbation functions // Proc. SPIE 10808, Photonics Applications in Astronomy, Communications, Industry, and High-Energy Physics Experiments 2018, 108082Y, doi: 10.1117/12.2501694.
31. Sergey I. Vyatkin, Sergii A. Romanyuk, Sergii V. Pavlov, and etc. Using lights in a volumeoriented rendering // Proc. SPIE 10445, Photonics Applications in Astronomy, Communications, Industry, and High Energy Physics Experiments 2017, 104450U; doi: 10.1117/12.2280982..
32. Oleg G. Avrunin; Maksym Y. Tymkovych; Sergii V. Pavlov; Sergii V. Timchik; Piotr Kisała, et al. Classification of CT-brain slices based on local histograms, *Proc. SPIE* 9816, Optical Fibers and Their Applications 2015, 98161J (December 18, 2015); doi:10.1117/12.2229040.
33. Olexander N. Romanyuk; Sergii V. Pavlov; Olexander V. Melnyk; Sergii O. Romanyuk; Andrzej Smolarz, et al. Method of anti-aliasing with the use of the new pixel model, *Proc. SPIE* 9816, Optical Fibers and Their Applications 2015, 981617 (December 18, 2015); doi:10.1117/12.2229013.
34. S. O. Romanyuk; S. V. Pavlov; O. V. Melnyk. New method to control color intensity for antialiasing. Control and Communications (SIBCON), 2015 International Siberian Conference. -